A 500kHz ZVS Class E Type DC-DC converter with Two Anti-Series MOSFETs Topology

Zhang Shu, *IEEE member*, Wang Chen, Yue Fengfa, Wang Yijie, *IEEE Senior Member,* Jose Marcos Alonso, *IEEE Fellow*

***Abstract*—Power converters powered by batteries have been widely used in many applications, such as outdoor emergency lighting, electric motorcycle charger, unmanned aerial vehicle supply and so on. This paper presents a 500 kHz zero-voltage-switching (ZVS) Class E type DC-DC converter with two anti-series MOSFETs used for battery-powered applications. The low-side MOSFET is adopted as the main switch to realize the working operation of traditional Class E resonant converter, while the high-side anti-series MOSFET is used to implement the regulation of the converter output voltage based on pulse width modulation (PWM). Both active switches are ZVS operated so that a high efficiency can be achieved. By changing the high-side MOSFET duty cycle, the ac voltage of the resonant tank is also changed to regulate the output voltage consequently. The control method is simple, and the operating frequency is constant, which is beneficial for the design of the resonant components. A 100-W prototype is built to verify the validity of the proposed control method for which a 94.85% efficiency has been achieved.**

***Index Terms*—Anti-series MOSFET, Class E converter, DC-DC converter, resonant converter.**

NOMENCLATURE

V_{in}	Input voltage;
I_f	DC input current flowing in L_f;
I_R	Amplitude of resonant current i_r;
$L_f (L_{f2})$	Choke inductance;
S_1	Low-side power MOSFET switch;
S_2	High-side power MOSFET switch;
L_r	Resonant inductance;
C_r	Resonant capacitance;
C_o	Output capacitance;
R_{ac}	Equivalent *AC* resistance;
R_{dc}	Equivalent *DC* resistance;
v_{ds1}	Drain-source voltage of S_1;
v_{ds2}	Drain-source voltage of S_2;
v_{cr}	Voltage across C_r;
v_{Rac}	Voltage across R_{ac};
v_{Lb}	Voltage across L_b;
v_s	Total voltage across both switches (v_{ds1}-v_{ds2});
v_{sm1}	Fundamental voltage of v_s;
V_{Rac1}	Fundamental voltage of v_{Rac};
V_{Lb1}	Fundamental voltage of v_{Lb};
C_{s1}	Drain-source capacitance of S_1;
C_{s2}	Drain-source capacitance of S_2;
i_{cs1}	Current flowing through capacitor C_{s1};
i_{cs2}	Current flowing through capacitor C_{s2};
i_r	Current into the resonant tank;
D_{r1}	Output rectifier diode;
D_{b2}	Diode of S_2;
Q_L	Quality factor;
ω	Angular switching frequency ;
φ	Initial angle of the resonant current;
θ	Conduction angle;
PWM_1	Drive signal of switch S_1;
PWM_2	Drive signal of switch S_2;
P_{sw}	Switch conduction loss;
I_{rms}	RMS current through the switch;
$R_{ds(on)}$	Drain-source branch resistor;
P_d	Diode conduction loss;
I_{fd}	Forward RMS current through diode;
V_{fd}	Forward voltage through diode;
P_r	Resonant tank conduction loss;
$I_{r,rms}$	RMS current in resonant tank;
R_r	Equivalent resonant resistance.

I. INTRODUCTION

OWING to the increasing demand of high-power density battery-powered supplies in many applications, such as mobile phones or pad chargers, Personal-Computer (PC) power adapters, unmanned aerial vehicles, and so on, more and more applications need a small volume power supply [1-3]. The adoption of high switching frequency can decrease the volume of passive components but decreasing switching loss, has naturally become the next interesting target of dc-dc converter design. Compared to conventional dc-dc converters, such as Buck, Buck-Boost, SEPIC and so on, resonant converters which utilize the resonance of an inductor and a capacitor can realize Zero-Voltage-Switching (ZVS) or Zero-Current-Switching operations (ZCS)[4-7]. Therefore, in high-frequency applications, resonant converters have become a priority scheme.

In high-power applications, the Dual-Active-Bridge (DAB) converter with an LC or CLLC resonant cell has been widely used with all switches under soft-switching operation [8-10]. For the DAB converter, a complex control method, for example, dual-phase-shift, triple-phase-shift, model predictive control, etc., is definitely adopted to satisfy the full-load soft-switching characteristic. In low-medium power applications, LLC converter is the common resonant converter which can achieve the primary-side ZVS for the controlled switches, and secondary-side diode ZCS characteristic. But when switching frequency becomes higher than resonant frequency, especially at light-load condition, the secondary-side ZCS characteristic disappears. Moreover, the two converters above contain more components, which increases the system cost [11-13]. Besides the above-mentioned resonant converters, in high-frequency applications, the Class E type converter has some obvious advantages [14-16]: simple structure, ZVS switching feature, current-fed, low current ripples. There are more and more applications adopting the Class E resonant converter, such as radio-frequency power amplifiers, wireless power transfer, LED drivers, dc-dc bidirectional converters, etc. [17-19]. Like other resonant converters, a Pulse-Frequency-Modulation (PFM) control method is used to regulate the output voltage while the duty cycle is kept constant at 0.5 for the Class E converter. At rated working condition, the Class E converter has an excellent performance. However, at light-load condition, the changing of the switching frequency to satisfy the demand of voltage or output power, makes it difficult to design the resonant inductor and capacitor. If the switching frequency remains unchangeable, a nominal resonant working condition will be held. Generally, a PWM method is a candidate to replace the PFM control method. In [19], a PWM method is proposed to regulate a Class E converter which provides some improvement for expanding the operation range. Obviously, having only an active switch makes it too difficult to regulate the converter in a wide load range. To draw a conclusion, only one active switch restricts the regulation performance of the Class E resonant converter.

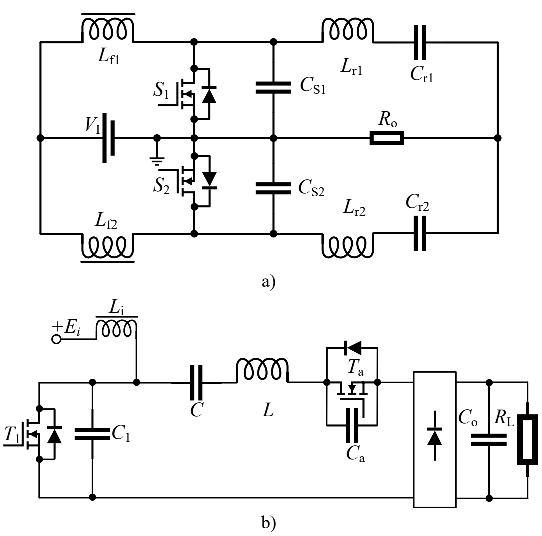

Fig.1 Previous Class E circuit: a) converter proposed in [20], b) converter proposed in [21]

In [20], two identical Class E circuits are combined into one topology as shown in Fig.1 a). In this structure, a phase-shift control method is adopted to regulate the output current. The control method remains the conventional Class E operation mode, and it is simple to implement without complex control logic. However, more passive components are needed in the circuit and the selection of identical specifications increases the design complexity. In [21], an active switch is series-connected in the resonant tank cell as shown in Fig.1 b). By changing the resonant frequency of the resonant tank, the output voltage is controlled. This method holds the switching frequency constant to simplify the design of resonant components. But the soft-switching state is influenced, that is to say, ZVS operation is lost. In [22], by resetting the position of the active switch, and still changing the resonant frequency of the resonant tank, the active switch is also used as rectifier to control the output voltage. However, the ZVS state is still influenced.

In this paper, an innovative technique is presented, in which an anti-series active switch is placed to enhance the main active switch. By using Pulse-Width-Modulation (PWM) control, the drain-to-source voltage of the whole two-MOSFET switch is changed to regulate the output voltage. The contributions of this paper can be stated as follows:

1) The switching frequency of the two active switches is constant. This way, this method can simplify the design of resonant passive components.

2) The high-side switch is modulated in PWM scheme, which is easy to implement. Meanwhile, the low-side switch is operated with 0.5 duty cycle and constant working frequency, which does not change nominal working state of the traditional Class E converter and keeps ZVS feature.

3) Utilizing the body diode, or an added diode, of the high-side switch, the anti-series active switch works either as a switch or as a diode, which decreases the switch driving loss.

This paper is organized as follows. In Section II, the working principle of the proposed Class E converter is discussed in detail. The analysis and design of the Class E resonant converter are elaborated in Section III. An experimental prototype is built to show the results of the proposed Class E resonant converter in Section IV. Finally, a conclusion is drawn in Section V.

II. WORKING PRINCIPLE OF PROPOSED CLASS E CONVERTER

The proposed two-switch anti-series Class E converter is shown in Fig.2. It contains four function cells. First, the input cell consists of the input source and a choke inductor, which provides a constant current source; Second, anti-series two active switches are the control cell to regulate the output voltage; Third, the resonant tank is made up by a resonant inductor and a capacitor; Lastly, a half-wave or full-wave rectifier is connected to the resonant tank to supply the load.

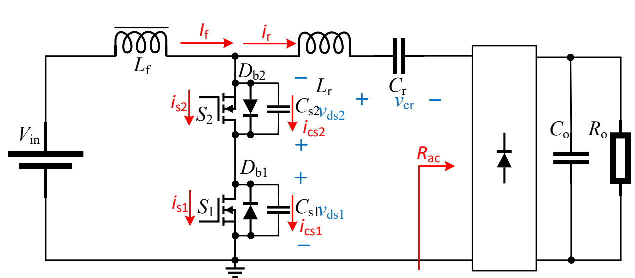

Fig.2 Proposed anti-series two-switch Class E dc-dc converter.

The principle of the proposed Class E converter is discussed as follows:

1) Period [0: θ_1]: At the beginning, S_1 is turned off and S_2 is driven on. The drain-source voltage v_{ds1} is increasing. Meanwhile, the current i_{cs1} begins to decrease from the

instantaneous peak value. At angle θ_1, current i_{cs1} changes its flowing direction, therefore the drain-source voltage v_{ds1} reaches the peak value. The resonant current flow loop is C_r-L_r-S_2-C_{s1}-R_{ac}, as shown in Fig.3 a).

2) Period [θ_1: θ_2]: S_2 is still turned on. The drain-to-source voltage of switch S_2 retains zero clamped by S_2. But the voltage v_{ds1} begins to decrease from the peak value. Meanwhile, current i_{cs1} increases in reverse direction, as shown in Fig.3 b). At angle θ_2, S_2 is turned off.

3) Period [θ_2: θ_3]: When S_2 is turned off, C_{s2} begins to be charged by resonant current i_r and C_{s1} begins to discharge to C_{s2}. Therefore, v_{ds2} begins to increase from zero and v_{ds1} continues to decrease. Because both switches S_1, S_2 are turned off, the resonant current flow loop is C_{s1}-C_{s2}-L_r-C_r-R_{ac}, as shown in Fig.3 c). At angle θ_3, the v_{ds1} reaches zero.

The resonant current i_r is depicted in (1). According to Kirchhoff's current law, (2) can be obtained.

$$i_r(\theta) = I_R \sin(\theta - \varphi) \tag{1}$$

$$\begin{aligned} I_f &= i_{cs1} + i_r \\ &= i_{cs1}(\theta) + I_R \sin(\theta - \varphi) \end{aligned} \tag{2}$$

During the period [0: θ_3], the expression v_{ds1} is shown in (3).

$$\begin{aligned} v_{ds1}(\theta) &= \frac{1}{\omega C_{s1}} \int_0^{\theta} i_{cs1}(\xi) d\xi \\ &= \frac{1}{\omega C_{s1}} \int_0^{\theta} I_f - I_R \sin(\xi - \varphi) d\xi \\ &= \frac{1}{\omega C_{s1}} \left\{ I_f \cdot \theta + I_R [\cos(\theta - \varphi) - \cos\varphi] \right\} \end{aligned} \tag{3}$$

4) Period [θ_3: θ_4]: v_{ds2} still increases, meanwhile current i_{cs2} decreases gradually. When i_{cs2} reaches zero, v_{ds2} attains its peak value. Then, i_{cs2} changes the flowing direction to increase, and v_{ds2} begins to decrease. Because S_1 is clamped by the D_{b1}, v_{ds1} holds zero. At angle θ_4, S_1 is turned on. Because v_{ds1} remains zero, the ZVS soft-switching characteristic is achieved.

5) Period [θ_4: θ_5]: i_{cs2} continues to increase, at angle θ_5, v_{ds2} reaches zero too. As shown in Fig.3 e), by changing the duty cycle D_2 of switch S_2, the whole voltage v_s = (v_{ds1} −v_{ds2}) also changes. In next Section III, the relationship between V_{Rac} and v_s will be discussed.

During the period that θ belongs to [θ_2: θ_5], voltage v_{ds2} is also obtained just like v_{ds1} deduction shown above, as given in (4).

$$v_{ds2}(\theta) = \frac{1}{\omega C_{s2}} \left\{ I_f \cdot (\theta - \theta_2) + I_R [\cos(\theta - \varphi) - \cos(\theta_2 - \varphi)] \right\} \tag{4}$$

6) Period [θ_5: θ_6]: S_1 is still turned-on, so the voltage v_{ds1} is zero. The anti-series switch S_2 is also clamped by diode D_{b2}, so v_{ds2} is also zero. At angle θ_6, another new cycle begins.

Because the stored energy in the choke inductor L_f is zero in one switching cycle, the input voltage V_{in} is the average value of the two anti-series switch voltage v_s. According to (3) and (4), V_{in} is determined in (5).

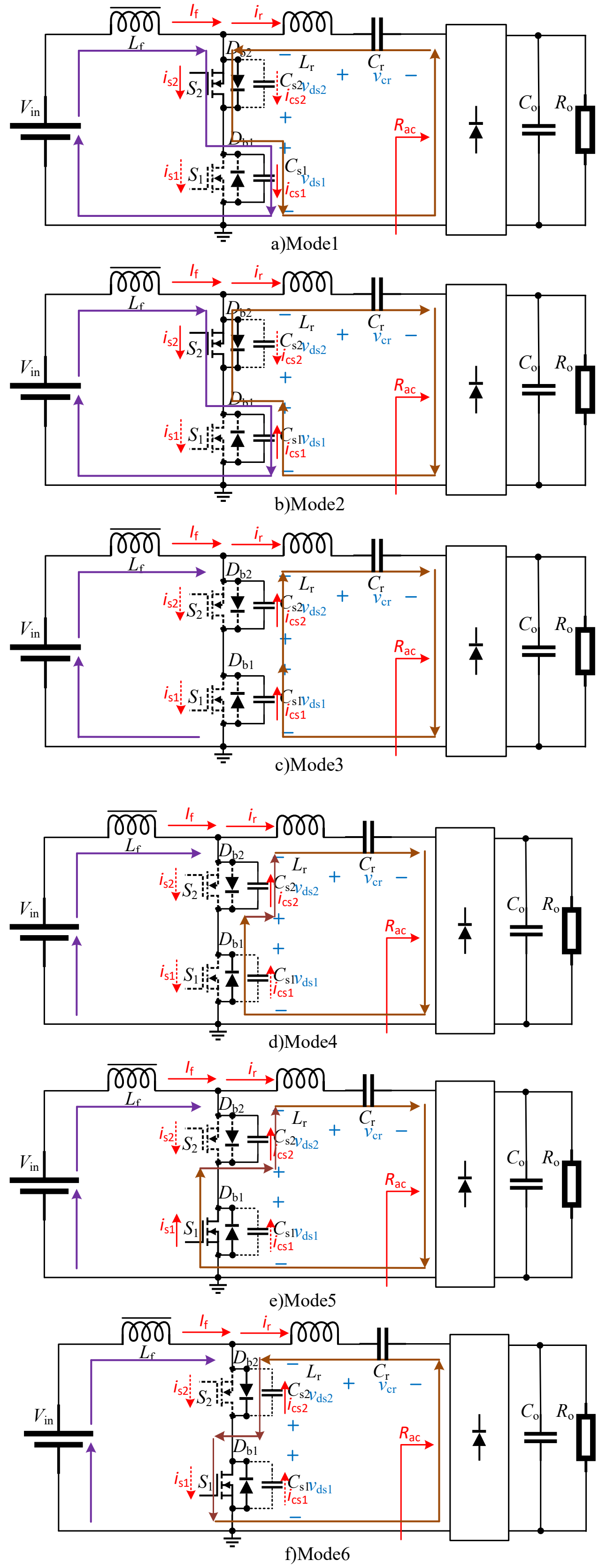

Fig.3 Working Modes of proposed Class E dc-dc converter.

$$V_{in}=\frac{1}{2\pi}\int_0^{2\pi}(v_{ds1}-v_{ds2})d\theta$$
$$=\frac{1}{2\pi}[\int_0^{2\pi}v_{ds1}d\theta-\int_0^{2\pi}v_{ds2}d\theta] \quad (5)$$
$$=\frac{1}{2\pi}[\int_0^{\theta_3}v_{ds1}(\xi)d\xi-\int_{\theta_2}^{\theta_5}v_{ds2}(\xi)d\xi]$$

The main waveforms of voltage and current in the topology are shown in Fig.4. v_{ds1} and v_{ds2} both have ZVS characteristics. When the duty cycle D_2 changes, v_{ds2} also changes, that is to say, v_s will also change to regulate the ac voltage v_{Rac}. The detailed deduction is discussed in the following section.

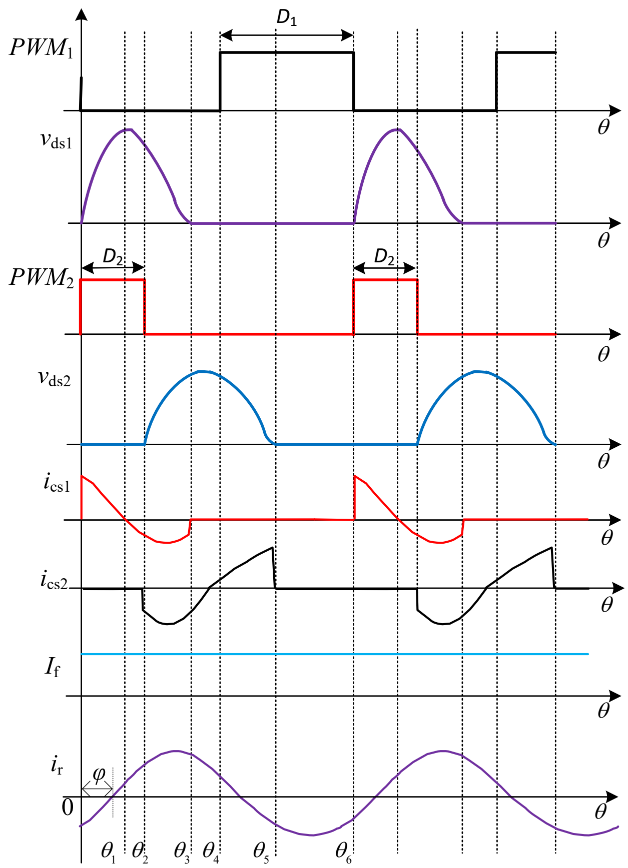

Fig.4 Main Waveforms of proposed Class E dc-dc converter.

III. PERFORMANCE ANALYSIS AND NUMERICAL SOLUTIONS

To simplify the circuit performance analysis, the following conditions are assumed:

1) The choke inductor is so large that the ac current is negligible compared with the dc current.

2) The diodes and MOSFETs are ideal to operate with instant turn on and turn-off. The drop voltage is also ignored.

3) The resonant current is close to the sinusoidal waveform. So, the quality factor is set higher than 2.5.

For the resonant inductance L_r, it can be divided into two parts: inductances L_a and L_b. L_a joins the resonance with the capacitance C_r. L_b provides the weak inductance which does not join in the resonance. For the traditional Class E converter, the switching frequency ranges from f_{r1} to f_{r2}. F_{r1} is the resonance frequency of L_r and C_r, and f_{r2} is the resonance frequency of L_r, C_r and drain-source capacitor C_s. For the proposed Class E converter, the new f_{r2} is higher than the value discussed above owing to the new drain-source capacitor C_{s2}. Therefore, the real inductor L_r is a little higher than the theoretical result. In (6), the relation among L_a, L_b and C_r is shown.

$$Q_L=\frac{\omega L_r}{R_{ac}}=\frac{\omega(L_a+L_b)}{R_{ac}}=\frac{1}{\omega C_r R_{ac}}+\frac{\omega L_b}{R_{ac}} \quad (6)$$

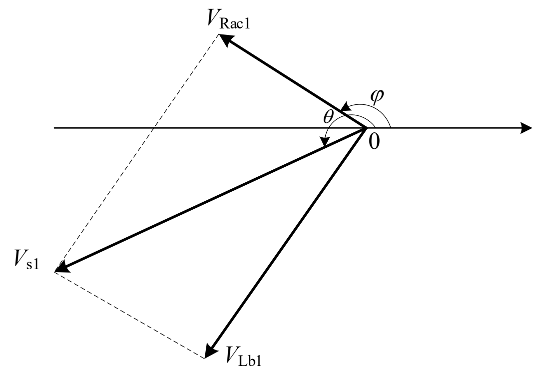

Fig.5 Vector diagram of voltage fundamental component.

In order to calculate the numerical solutions, the conduction angle boundary is set to satisfy the nominal working condition. $\theta_2 = 2\pi D_2$, $\theta_3 = \pi$, $\theta_5 = \frac{3}{2}\pi$ are set, then V_{in} is further expressed in (7).

$$V_{in}=\frac{(4\sin\varphi-2\pi\cos\varphi)\cdot I_R+\pi^2\cdot I_f}{4\pi\omega C_{s1}}-\frac{(4\pi D_2-3\pi)^2\cdot I_f}{16\pi\omega C_{s2}}$$
$$-\frac{[4\pi D_2\cos(\varphi-2\pi D_2)-3\pi\cos(\varphi-2\pi D_2)]\cdot I_R}{4\pi\omega C_{s2}} \quad (7)$$
$$-\frac{[-2\cos\varphi+2\sin(\varphi-2\pi D_2)]\cdot I_R}{4\pi\omega C_{s2}}$$

In order to satisfy the ZVS condition of S_1, at angle θ_3, $v_{ds1} = 0$. Setting $\theta_3 = \pi$, the relation between I_f and I_R can be achieved in (8).

$$I_f=\frac{2\cos\varphi}{\pi}I_R \quad (8)$$

For the resonant tank, according to the fundamental analysis method, the ac voltage V_{Rac}, the whole switch voltage v_s and non-resonant inductor voltage v_{Lb} are deduced in (9) and (10).

$$V_{Rac}=\frac{1}{2\pi}\int_0^{2\pi}(v_{ds1}-v_{ds2})\sin(\theta-\varphi)d\theta$$
$$=\frac{1}{2\pi}[\int_0^{\pi}v_{ds1}\sin(\theta-\varphi)d\theta-\int_{\frac{\pi}{2}}^{2\pi}v_{ds2}\sin(\theta-\varphi)d\theta] \quad (9)$$

$$V_{Lb}=\frac{1}{2\pi}\int_0^{2\pi}(v_{ds1}-v_{ds2})\cos(\theta-\varphi)d\theta$$
$$=\frac{1}{2\pi}[\int_0^{\theta_3}v_{ds1}\cos(\theta-\varphi)d\theta-\int_{\theta_2}^{\theta_5}v_{ds2}\cos(\theta-\varphi)d\theta] \quad (10)$$

Substituting (3), (4) and (8) into (7), (9) and (10), the ac resistor R_{ac}, dc resistor R_{dc} and ωL_b can be obtained as shown in (11), (12) and (13). The resistance relationship can be calculated.

$$\begin{aligned}R_{dc} &= \frac{V_{in}}{I_f} = \frac{\sin\varphi}{2\omega\cos\varphi C_{s1}} \\ &- \frac{4\sin(\varphi-2\pi D_2)-4\cos\varphi+\pi(4D_2-3)^2\cos\varphi}{16\omega\cos\varphi C_{s2}} \\ &+ \frac{8\pi D_2\cos(\varphi-2\pi D_2)-6\pi\cos(\varphi-2\pi D_2)}{16\omega\cos\varphi C_{s2}}\end{aligned} \tag{11}$$

$$\begin{aligned}R_{ac} &= \frac{V_{ac1}}{I_R} = \frac{2\sin\varphi\cos\varphi}{\pi^2\omega C_{s1}} \\ &+ \frac{4\pi\cos\varphi-\pi^2(4D_2-3)^2\cos\varphi-4\pi\sin(\varphi-2\pi D_2)}{8\pi^2\omega C_{s2}} \\ &+ \frac{6\pi^2\cos(\varphi-2\pi D_2)-8\pi^2 D_2\cos(\varphi-2\pi D_2)}{8\pi^2\omega C_{s2}}\end{aligned} \tag{12}$$

$$\begin{aligned}\omega L_b &= \frac{V_{Lb1}}{I_R} = \frac{\pi^2-8\cos^2\varphi}{4\pi^2\omega C_{s1}} \\ &- \frac{(3-4D_2)\pi^2+(\pi-4)\sin(2\varphi)+4\pi(4D_2-3)\cos^2\varphi}{8\pi^2\omega C_{s2}} \\ &- \frac{4(\pi-2)\cos\varphi\cos(\varphi-2\pi D_2)-\pi\sin(2\varphi-4\pi D_2)}{8\pi^2\omega C_{s2}}\end{aligned} \tag{13}$$

According to (6), the resonant capacitor C_r can be calculated in (14).

$$C_r = \frac{1}{\omega\left(R_{ac}Q_L-\omega L_b\right)} \tag{14}$$

With the increase of Q_L, C_r is gradually decreasing. However, a smaller value means a higher voltage stress, as shown in (15). Therefore, the value of C_r is selected by considering a limited voltage stress.

$$\begin{aligned}V_{cr}(\theta) &= \frac{1}{\omega C_r}\int_0^{\theta} I_R\sin(\xi-\varphi)d\xi \\ &= \frac{1}{\omega C_r} I_R[\cos\varphi-\cos(\theta-\varphi)]\end{aligned} \tag{15}$$

In order to obtain ZVS operation, ωL_b should be higher than zero, which means a weak inductive behavior. According to (13), the relationship between φ and C_{s2}/C_{s1} for different values of D_2 is shown in Fig. 5. With the increase of D_2, the peak value of C_{s2}/C_{s1} decreases, at the condition that φ ranges from 0 to 90 degrees. The peak value of C_{s2}/C_{s1} is 1.5 times.

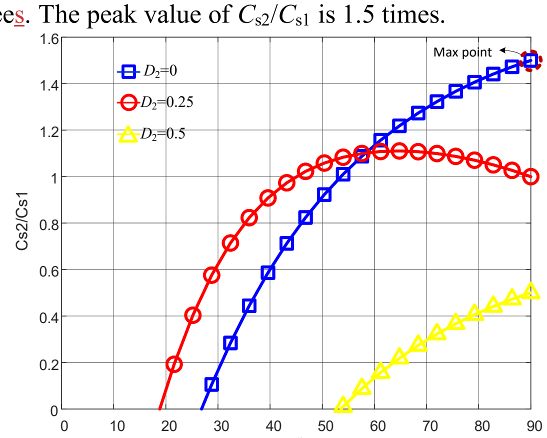

Fig.5 Relationship between C_{s2}/C_{s1} and φ at different D_2.

The equivalent circuit of the proposed resonant converter is shown in Fig.6. The secondary-side output circuit is simplified as a resistor R_{ac}. The Capacitors C_{s1}, C_{s2} are both included in the resonant loop.

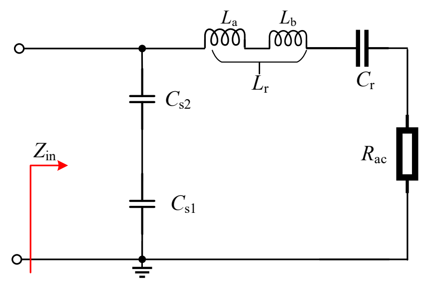

Fig.6 Equivalent circuit of proposed resonant converter

The input impedance $Z_{in}(s)$ is deduced in (16) whose Bode diagram is plotted in Fig. 7. An inductive range is determined which means a soft-switching characteristic. By increasing the value of C_{s2} to a limit value, the inductance range will not change. By decreasing value of C_{s2}, the soft-switching range narrows.

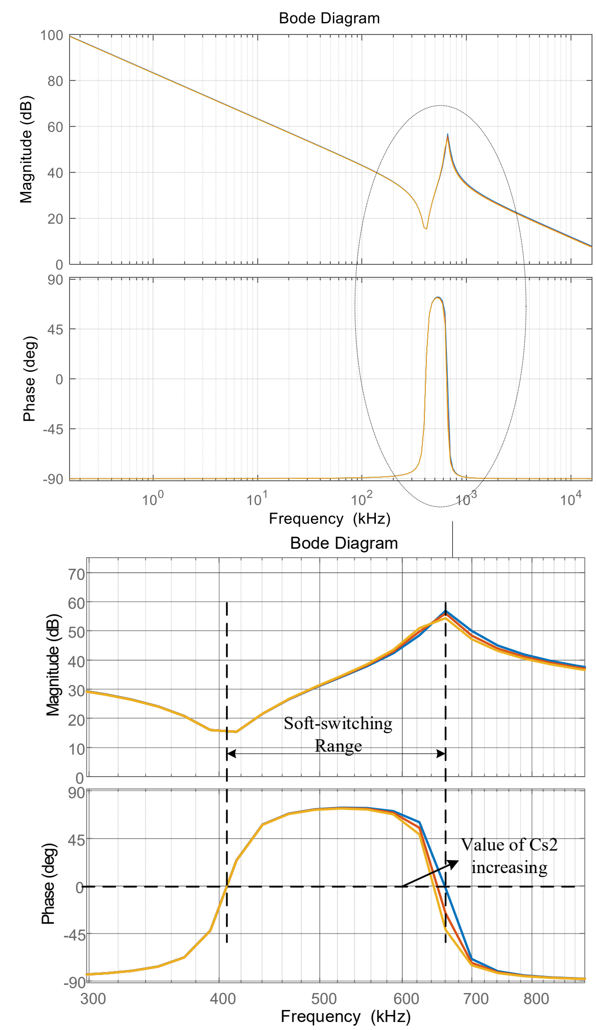

Fig.7 Bode diagram of input impedance $Z_{in}(s)$.

$$Z_{in}(s)=\frac{\left(\frac{1}{sC_{s1}}+\frac{1}{sC_{s2}}\right)\times(sL_r+\frac{1}{sC_r}+R_{ac})}{\left(\frac{1}{sC_{s1}}+\frac{1}{sC_{s2}}\right)+(sL_r+\frac{1}{sC_r}+R_{ac})} =\frac{\left(\frac{1}{sC_{s1}}+\frac{1}{sC_{s2}}\right)\times\left(L_rs^2+R_{ac}s+\frac{1}{C_r}\right)}{L_rs^3+R_{ac}s^2+(\frac{1}{sC_{s1}}+\frac{1}{sC_{s2}}+\frac{1}{C_r})s} \tag{16}$$

In order to guarantee the ZVS condition of S_1, the value of C_{s2} is higher than the one of C_{s1}, on the purpose of releasing all the energy stored in C_{s1}. The relation among Q_L, v_{ds1}, v_{ds2}, and v_{cr} is shown in Fig. 8. When the power quality factor Q_L increases, the peak voltage values of S_1, S_2 decrease as well. But the voltage stress of C_r is increasing sharply.

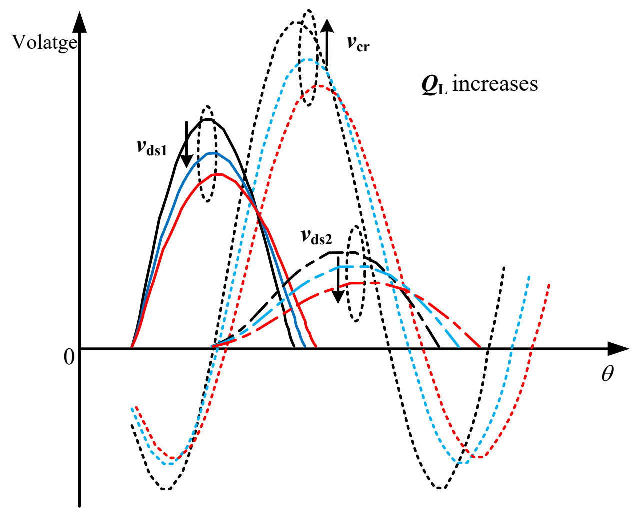

Fig.8 Relation among Q_L, v_{ds1}, v_{ds2}, and v_{cr}

For the capacitance C_r, a 3000 V rating voltage ceramic capacitor may satisfy the system requirements at a very high value of Q_L. But a higher rating voltage also increases the cost. High Q_L means a narrow-band signal selection, which restricts the energy in other frequency bands passing through the resonant tank to the load. Likewise, small Q_L means small value of L_r which increases the conduction loss, due to a high circulating current. According to (13) and (14), L_b and C_r can be calculated. Then, L_a is derived as shown in (17).

$$L_a=\frac{Q_LR_{ac}}{\omega}-L_b \tag{17}$$

The output stage can be generated by half-wave rectification or full-wave rectification. The relation between R_{ac} and R_o is depicted in (18), where n is the turn ratio of primary-side to secondary-side in the transformer. When a high gain of the system is demanded, a transformer is needed.

$$R_{ac}=\begin{cases}\frac{2}{\pi^2}R_o, & \text{half-wave rectifier}\\ \frac{8n^2}{\pi^2}R_o, & \text{full-wave rectifier}\end{cases} \tag{18}$$

Now, the gain M of the dc-dc converter is discussed as follows. The input power is shown in (19). The output power P_o is depicted in (20). The transmission efficiency is designated as η; then, M is calculated in (21).

$$P_{in}=V_{in}I_f=\frac{V_{in}^2}{R_{dc}} \tag{19}$$

$$P_o=V_oI_o=\frac{V_o^2}{R_o} \tag{20}$$

$$M=\frac{V_o}{V_{in}}=\sqrt{\eta\frac{R_o}{R_{dc}}} \tag{21}$$

The system gain M is related to the equivalent resistances R_o and R_{dc}. For a high-gain application, the rectification circuit can employ a transformer. According to (11), (12), (18), (21), M is a function of variable D_2 in (22). The relation between M and D_2 is depicted in Fig.9. When φ equals to 30°, M changes non-linearly with the D_2. When φ increases to 60°, the linearization becomes better which satisfies the application requirement. At different values of φ, the system M changes with the D_2; for example, at the condition of C_{s1} = 6.8 nF and C_{s2} = 12 nF, φ= 60°, M is 2 at the angle of D_2 = 0.3. The output power P_o is also regulated by D_2 which is depicted in (23).

$$M=\frac{V_o}{V_{in}}=\sqrt{\eta\cdot\frac{\pi^2}{2}\cdot\frac{R_{ac}}{R_{dc}}}=f\left(D_2\right) \tag{22}$$

$$P=\frac{V_o^2}{R_o}=\eta\frac{\pi^2}{2}\cdot\frac{R_{ac}(D_2)}{R_{dc}(D_2)}\cdot\frac{1}{R_o}\cdot V_{in}^2 \tag{23}$$

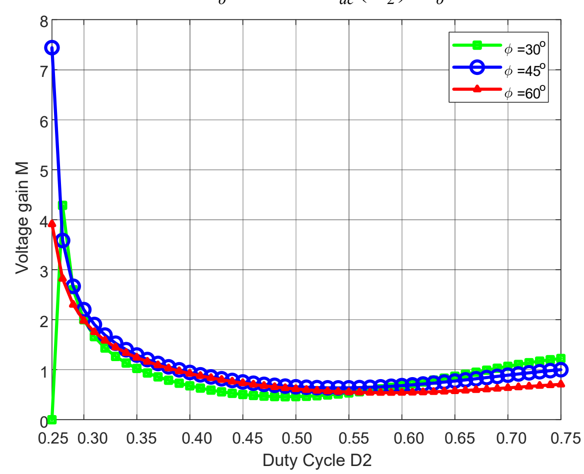

Fig.9 Relation of M and D_2 at different Q_L

The main parameters in this topology are L_r、 C_r、 C_{s1}、 C_{s2}. The basic parameter calculation procedure can be summarized as follows.

Firstly, the quality factor Q_L needs to be chosen as a suitable value. It influences the voltage stress and value of L_r. A high Q_L will increase the voltage stress of C_{s1} and C_{s2}, and a high value of L_r which is good for decreasing conduction loss. Therefore, it is a trade-off for stress and efficiency.

Secondly, once the power factor Q_L is determined, according to the definition of $Q_L=\left(\omega L_r\right)/R_{ac}$, the value of L_r can be calculated. In order to simplify the calculation, assuming that C_r resonates with L_r, a value of C_r can be obtained. In fact, part of L_r is definitely L_a which participates in resonance with C_r. Therefore, as a last step, the value of C_r should be revised.

Thirdly, in order to satisfy the ZVS characteristic of S_1, the input impedance seen from the switch S_1 can be deduced. The angle φ is higher than zero, the ZVS range can be achieved, and since a weak inductance is guaranteed, the condition of $\omega L_b > 0$ is also satisfied. Combining the voltage stress among C_{s2}, C_{s1} and C_r, the values of C_{s1} and C_{s2} can be achieved.

Finally, these values will influence the voltage gain. Further, the values of four components are done with minor correction.

IV. DESIGN CONSIDERATIONS AND COMPONENT SELECTION

In this paper, a 100 W prototype is built whose nominal input voltage is 48 V with a range from 30 Vdc to 60 Vdc, rated output voltage/current 50 V/2 A. And the switching frequency is 500 kHz for both S_1, S_2. The choke inductor L_f is calculated as shown in (24). The main specifications and parameters of the proposed converter are listed in Table I. A digital signal processor TMS320F28377 is adopted as the main controller.

$$L_f = 2(\frac{\pi^2}{4}+1)\frac{R_{ac}}{f_s} \tag{24}$$

Fig. 9 shows the schematic diagram of the laboratory prototype. The experimental prototype is shown in Fig.10. CoolMOS MOSFET IPP60R022S7 was selected to implement the active switches. The rectifier cell adopts the conventional Class E rectifier circuit which consists of one diode D_{r1}. D_{r1} is implemented by an ultra-fast recovery diode STPS20200C. In order to improve the current capability of S_2, a diode D_{b2} is connected in parallel with S_2. The resonant inductor L_r is set to 23 μH, and the resonant capacitor C_r consists of six 1 nF units and one 660 pF unit in parallel. Meanwhile five 2.2 μF capacitors in parallel are used to build the output capacitor C_o.

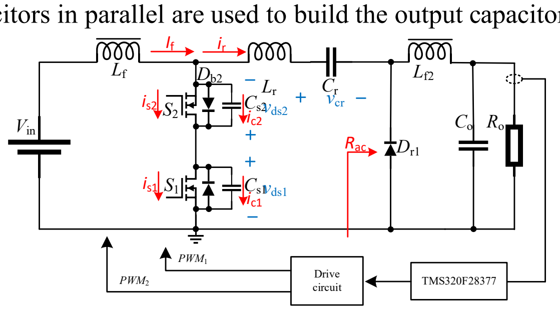

Fig.9 Schematic diagram of the laboratory prototype.

TABLE I
SPECIFICATION AND PARAMETERS OF PROPOSED CONVERTER

Component	Value	Device Models
L_f, L_{2f}	68 μH	WurthElektronik74437529203680
S_1, S_2	600V/23A	IPP60R022S7 Cool − MOS
L_r	23 μH	0.1mm ∗ 200P − 22Turns
C_r	6.66 nF	1 nF/3000V,660 pF/3000V
C_o	11 μF	2.2 μF/250V
D_{r1}, D_{b2}	200V/10A	STPS20200C
Drive IC		1ED3124MU12HXUMA1
Auxiliary Power		F0524S-2WR2

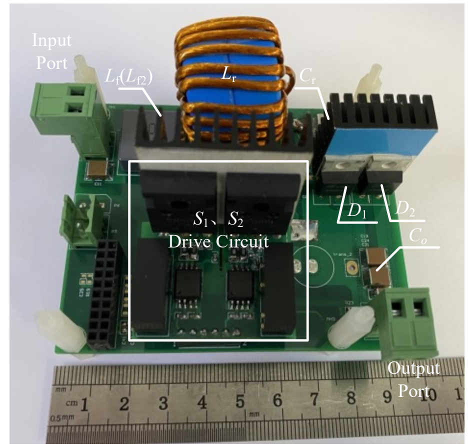

Fig.10 Experimental prototype of proposed converter topology.

At the rated output power, the waveform of V_{ds1} and V_{ds2} are shown in Fig.11. As can be seen, ZVS characteristic can be achieved.

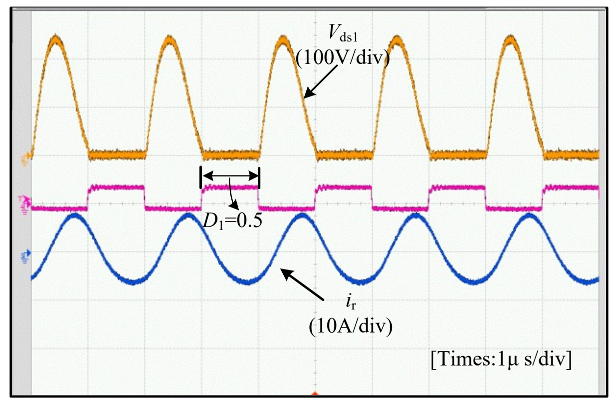

a)Drain-source voltage and drive signal of switch S_1

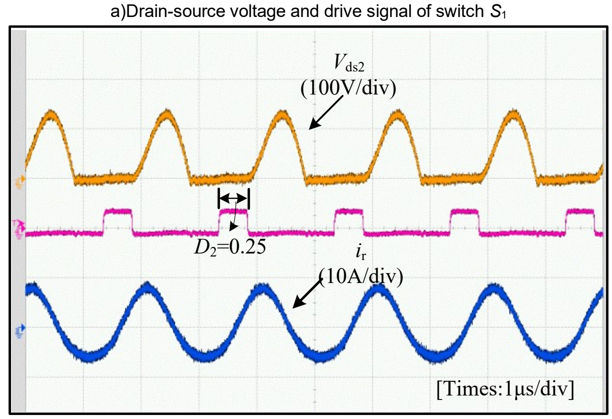

b)Drain-source voltage and drive signal of switch S_2

Fig. 11 Waveforms of drain-source voltage and drive signal in S_1 and S_2

By modulating the duty cycle of S_2, the output voltage can be regulated. When D_2 equals 0.5, the output voltage V_o is changed as illustrated in Fig. 12. By adjusting D_2, the output voltage and current is also changed. Because the duty cycle D_1 is 0.5 constant, V_{ds1} is still under ZVS operation. At the condition of D_2=0.7, V_{ds2} changes to nearly zero, as depicted in Fig. 13. The output voltage is regulated by changing the voltage V_{ds2} adopting the PWM method.

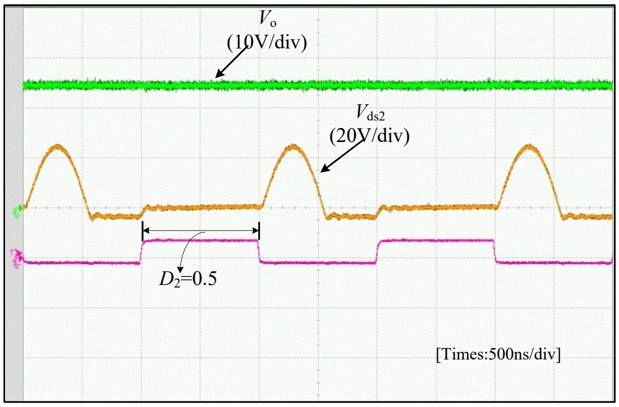

Fig. 12 Waveforms of V_{ds2} and output voltage at D_2=0.5.

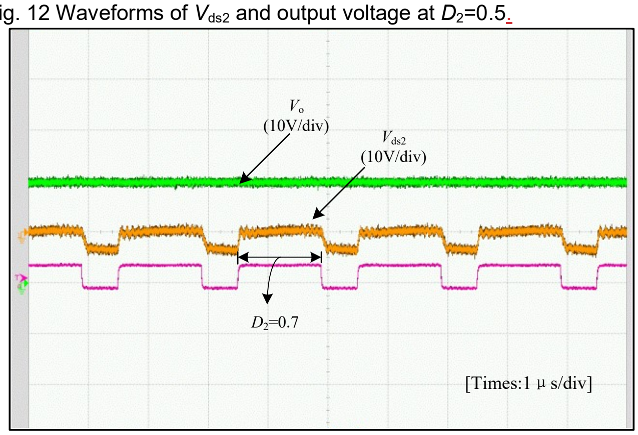

Fig. 13 Waveforms of V_{ds2} and output voltage at D_2=0.7.

The waveforms of current in L_f and input voltage V_{in} are shown in Fig.14. The ripple in current is rather small so that the input port is regarded as a constant current source.

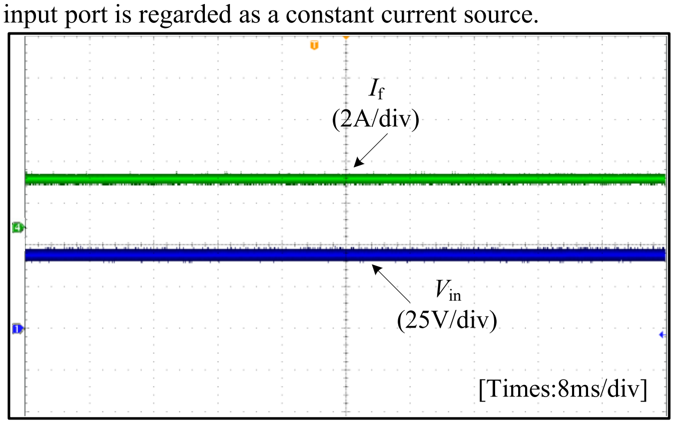

Fig. 14 Waveforms of input voltage V_{in} and current I_f.

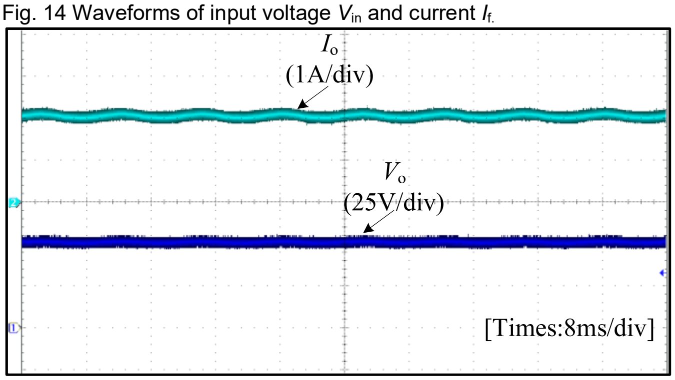

Fig. 15 Waveforms of output voltage V_o and current I_o.

The waveforms of output voltage and current are shown in Fig. 15 at the rated working condition. Fig. 16 shows the waveform of v_{cr} which demonstrates that a low rating voltage capacitor can be adopted for C_r.

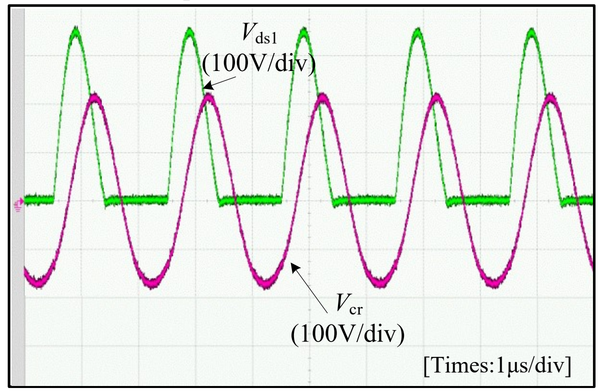

Fig. 16 Waveforms of resonant capacitor C_r voltage V_{cr} and V_{ds1} at the rated condition.

Fig. 17 shows the system loss breakdown at rated output power. The system loss mainly contains MOSFET loss (including conduction and switching loss), magnetic loss, and diode loss (rectifier loss and reverse recovery loss). Because the proposed converter has soft-switching characteristic, the loss of the switch is the conduction loss. Using (25), the switch loss P_{sw} can be calculated. Owing to the fact that an ultrafast recovery diode is adopted, the reverse recovery loss is neglected. Using (26), the conduction loss in a diode can be obtained.

$$P_{sw} = I_{ds,rms}^2 \cdot R_{d(on)} \tag{25}$$

$$P_d = I_{fd} V_{fd} \tag{26}$$

Because the value of L_f reaches mH level, the resistor is relatively high which cannot be ignored. The series resistance loss in L_f is shown in (27).

$$P_f = I_{f,rms}^2 \cdot R_f \tag{27}$$

Resistive loss P_r in the resonant tank is calculated in (28). R_r is the equivalent resistance in resonance tank.

$$P_r = I_{r,rms}^2 \cdot R_r \tag{28}$$

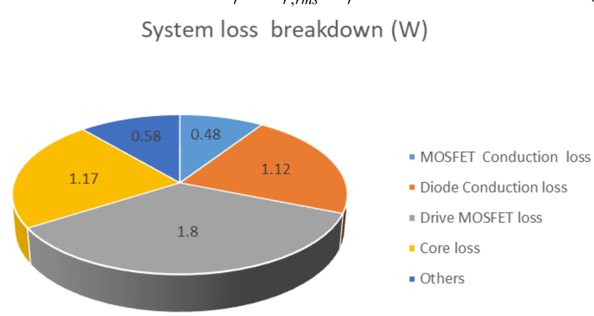

Fig.17 System loss breakdown at rated output power

Lastly, the magnetic loss is discussed in detail. The magnetic material is NPX106019, which has 23.232 uH at a current of 0 A and 22.7 uH at a current of 10 A. The volume of magnetic core is 4.154cm^3 and cross-sectional area of magnetic core Ae is 0.654cm^2. The relationship between core loss P_{cv} and flux density B is shown in Fig.18.

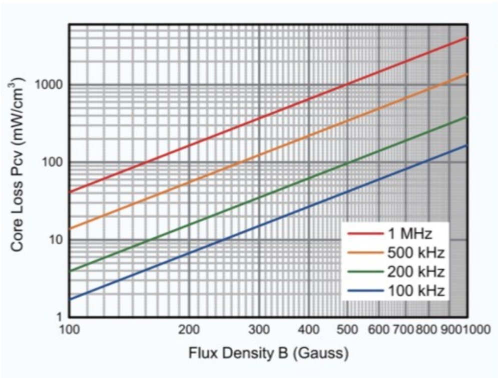

Fig.18 Relation between core loss P_{cv} and flux density B.

Fig.19 shows the efficiency curve at different output powers. The peak efficiency can reach 94.85% at rated output power. Moreover, at different output power, the efficiency is higher than 84%.

The comparison among the existing converters based on Class E circuit is shown in Table II. This research works adopt constant switching frequency. [20] mirrors Class E converter which eases the control method by phase shift method, but it has more components which increase the cost and decrease the power density. [22] adopts a new switch used as a rectifier diode to change the output voltage which also increases the system cost. [23] proposes a combined structure of Class DE and Class E which is regulated by phase shift method. But it still has no cost-advantage.

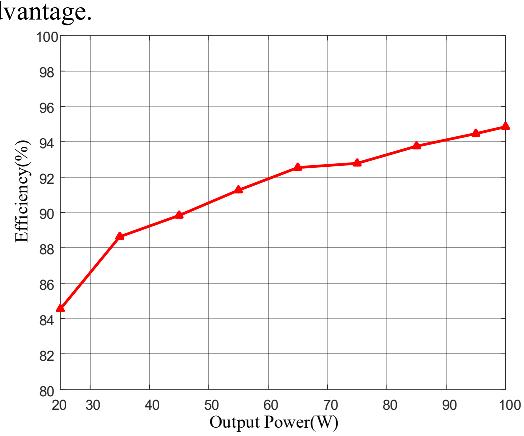

Fig.19 Efficiency curve of Class E converter at different output power

TABLE II
Comparison of other research works and proposed converter

		[20]	[22]	[23]	Proposed converter
Number of Components	Switches	2	3	2	2
	Diodes	2	2	1	1
	Caps	4	2	3	2
	Inductors	5	2	2	3
Switching frequency		500kHz	1MHz	1MHz	500kHz
Power		12W	22.5W	2.5W	100W
Efficiency		/	/	84%	94.5%
Control method		Phase Control	Controlled-Cap	Phase Control	PWM

V. Conclusion

This paper proposed a 500 kHz anti-series two-switches Class E dc-dc converter. It has some advantages of constant working switching frequency and easy regulation of the output voltage. The proposed technique makes it possible to increase the operating frequency, thus allowing for an improvement of the converter power density. By changing the duty cycle of the additional switch D_2, ZVS operation for both active switches is achieved. Meanwhile the traditional Class E operation mode is not changed, and the components are easy to design.

The improvement of the proposed converter can be summarized as follows.

First, anti-series two switches structure can be integrated into one module which is good for high frequency working. The drive circuit is able to be added into this module. The parasitic capacitor and inductor have the least influence on high frequency drive.

Second, the control method can be simplified. Especially in resonant converter, duty cycle of low-side switch can be kept constant; an oscillating circuit (high frequency) can be utilized instead of a drive signal and drive IC. By regulating the high-side switch, the output voltage can be controlled. Moreover, two switches can be? extended to phase shift control method.

Thirdly, the high-side switch keeps zero-voltage-switching characteristic, which is also good for high frequency application.

Finally, at the rated 100 W working condition, the peak efficiency can reach 94.85%. However, in order to increase the system voltage gain, a transformer has better to be added.

It is also fair to highlight some drawbacks of the proposed converter . The high-side switch needs to adopt an isolated drive circuit, and the body diode of the high-side switch must be capable of handling the large resonant current. Normal Si-based MOSFETs are not competent. Wide band gap devices have more advanced thermal characteristic, high-frequency switching characteristic, higher withstanding voltage, etc. Therefore, adopting SiC or GaN device is the next research direction. In addition, magnetic design is another aspect to improve, which highly contributes to increase power density and efficiency.

Acknowledgment

This work was supported by the Central University Basic Research Fund of China for the Central Universities (CAUC) under Grant No.3122019038.

References

[1] O. Karimzada, T. Uchida, and T. Masuda, et.al. "Design of a dc-dc converter using sic trench mosfets for ev fast chargers," in Proc. *2020 IEEE Workshop on Wide Bandgap Power Devices and Appl. in Asia*, pp. 1–5, 2020.
[2] Z. Zhang, F. Wang, and L. M. Tolbert, et.al. "Evaluation of switching performance of sic devices in pwm inverter-fed induction motor drives," *IEEE Trans. on Power Electron.*, vol. 30, no. 10, pp. 5701–5711, 2015.
[3] K. Yang, H. Qian, and M. Cai, et.al. "Optimization of high power density ac-dc converter based on silicon carbide device for uav," in Proc. *2019 22nd Inter. Conf. on Electrical Machines and Systems (ICEMS)*, pp. 1–6, 2019.
[4] T. Jiang, J. Zhang, and X. Wu, et.al. "A bidirectional llc resonant converter with automatic forward and backward mode transition," *IEEE Trans. on Power Electron.*, vol. 30, no. 2, pp. 757–770, 2015.

[5] T. Yao, Y. Guan, and F. Li, et.al. “A novel ac/dc converter based on stacked boost circuit and dual-mode llc circuit,” *IEEE Trans. on Indu. Appl.*, vol. 56, no. 6, pp. 6576–6585, 2020.
[6] Y. Wang, Y. Guan, D. Xu, and W. Wang, “A clcl resonant dc/dc converter for two-stage led driver system,” *IEEE Trans. on Indu. Electron.*, vol. 63, no. 5, pp. 2883–2891, 2016.
[7] J. Deng, S. Li, and S. Hu, et.al. “Design methodology of llc resonant converters for electric vehicle battery chargers,” *IEEE Trans. on Vehicular Technology*, vol. 63, no. 4, pp. 1581–1592, 2014.
[8] L. Wang, Q. Zhu, W. Yu, and A. Q. Huang, “A medium voltage bidirectional dc-dc converter combining resonant and dual active bridge converters,” in Proc. *IEEE Applied Power Electron. Conf. and Exposition (APEC)*, pp. 1104–1111, 2015.
[9] Z. Xiao, Z. He, and H. Wang, et.al. “General high-frequency-link analysis and application of dual active bridge converters,” *IEEE Trans. on Power Electronics*, vol. 35, no. 8, pp. 8673–8688, 2020.
[10] J. Everts, F. Krismer, and J. Van den Keybus, et.al. “Optimal zvs modulation of single-phase single-stage bidirectional dab ac–dc converters,” *IEEE Trans. on Power Electron.*, vol. 29, no. 8, pp. 3954–3970, 2014.
[11] Y. Wang, S. Zhang, and J. M. Alonso, et.al. “A single-stage led driver with high-performance primary-side-regulated characteristic,” *IEEE Trans. on Circuits and Systems II: Express Briefs*, vol. 65, no. 1, pp. 76–80, 2018.
[12] G. G. Pereira, M. A. Dalla Costa, and J. M. Alonso, et.al. “Led driver based on input current shaper without electrolytic capacitor,” *IEEE Trans. on Indu. Electron.*, vol. 64, no. 6, pp. 4520–4529, 2017.
[13] X. Xie, J. Wang, and C. Zhao, et.al. “A novel output current estimation and regulation circuit for primary side controlled high power factor singlestage flyback led driver,” *IEEE Trans. on Power Electron.*, vol. 27, no. 11, pp. 4602–4612, 2012.
[14] S. Zhang, Y. Qiu, and Y. Wang, et.al. “A high-power-factor integrated-stage ac-dc led driver based on flyback-class e converter,” in Proc. *IEEE Indu. Appl. Society Annual Meeting*, pp. 1–5, 2017.
[15] N. Bertoni, G. Frattini, and R. G. Massolini,et.al. “An analytical approach for the design of class-e resonant dc–dc converters,” *IEEE Trans. on Power Electron.*, vol. 31, no. 11, pp. 7701–7713, 2016.
[16] Y. Li, X. Ruan, and L. Zhang, et.al. “Optimized parameters design and adaptive duty-cycle adjustment for class e dc–dc converter with on-off control,” *IEEE Trans. on Power Electron.*, vol. 34, no. 8, pp. 7728–7744, 2019.
[17] M. Liu, M. Fu, and C. Ma, “Parameter design for a 6.78-mhz wireless power transfer system based on analytical derivation of class e current-driven rectifier,” *IEEE Trans. on Power Electron.*, vol. 31, no. 6, pp. 4280–4291, 2016.
[18] A. Mediano and N. O. Sokal, “A class-*e* rf power amplifier with a flat-top transistor-voltage waveform,” *IEEE Trans. on Power Electron.*, vol. 28, no. 11, pp. 5215–5221, 2013.
[19] S. Zhang, X. Liu, and Y. Guan, et.al. “Modified zero-voltage-switching single-stage LED driver based on Class E converter with constant frequency control method,” *IET POWER ELECTRON.*, vol. 11, iet-pel.2018.5155, no. 12, pp. 2010–2018, OCT, 2018.
[20] C.-Q. Hu, X.-Z. Zhang, and S.-P. Huang, “Class-e combined-converter by phase-shift control,” in Proc. *20th Annual IEEE Power Electron. Specialists Conf.*, pp. 229–234 vol.1, 1989.
[21] W.-J. Gu and K. Harada, “A new method to regulate resonant converters,” *IEEE Trans. on Power Electron.*, vol. 3, no. 4, pp. 430–439, 1988.
[22] Y.-F. Liu and P. Sen, “New class-e dc-dc converter topologies with constant switching frequency,” *IEEE Trans. on Indu. Appl.*, vol. 32, no. 4, pp. 961–969, 1996.
[23] H. Sekiya, S. Nemoto, Jianming Lu and T. Yahagi, "Phase control for resonant DC-DC converter with class-DE inverter and class-E rectifier," *IEEE Trans. on Circuits and Systems I: Regular Papers*, vol. 53, no. 2, pp. 254-263, Feb. 2006.